The Space-Time-Averaging Procedure and Modeling of the RF Discharge, Part II: Model of Collisional Low-Pressure RF Discharge

Igor D. Kaganovich and Lev D. Tsendin

Abstract — **A self-consistent equations system for the low-pressure RF discharge is formulated and qualitatively analyzed. If the plasma and sheath dimensions exceed the electron-energy relaxation length, a simple spatially averaged kinetic equation can be derived that resembles the conventional one for the local case. Since the energy-diffusion coefficient for the slow electrons that are trapped by the average electric field in the discharge center is small, the distribution function slope decreases significantly with the energy growth. Analytic estimates are derived and reasonable agreement with the experiments of Godyak is obtained.**

I. Introduction

In Part I of this study [1], the time-averaging over fast-electron-motion method was proposed for the description of the self-consistent stationary electric field which determines the ion motion and plasma profile in RF discharge at medium and high pressures. The oscillatory field $\tilde{E}(x,t)$ was determined by the ion profile and RF current-conservation condition. Since in this case the characteristic scale was large compared with the electron-energy relaxation length, the electron distribution function (EDF) and excitation and ionization rates in any given point depend on the local value of $\tilde{E}(x,t)$. Therefore it was possible to use numerous results of the EDF calculations in spatially homogeneous RF fields.

The case of low-pressure RF discharge is far more complicated. The main difficulty is connected with the effects of nonlocality that are significant in He, for example, at pL_0 values as high as ~ 10 torr cm [2]. Existing analytic estimates [3] are based on rather crude assumptions about the plasma profile and do not permit the quantitative comparison with experiment. The EDF in this case, even in the simplest plane-parallel geometry, becomes a complicated function of four arguments: time, spatial coordinate x, and two velocity components, v_x and $v_\perp$. Since the stationary and oscillatory fields are to be calculated self-consistently, a straightforward numerical approach even for simplified models becomes an extremely troublesome problem [4]–[8]. The necessity of a relatively simple theory that would permit calculating self-consistently field and plasma density profiles and the EDF is greatly stimulated by recent experiments [9] where the EDF in the central plane of the RF discharge was investigated and the considerable enrichment of the EDF low-energy part was observed in the nonlocal regime. We shall demonstrate here how spatial and temporal averaging [1] that analytically excludes fast motions can lead to considerable simplifications in the nonlocal case also.

The electronic motion is characterized by several frequency scales: RF field frequency ω, electron-transport collision frequency $\nu = n_a v \sigma$, inelastic collision frequency $\nu^* = n_a v \sigma^*$, electron plasma frequency ω_{0e}, and electron bounce frequency $\Omega_b = v/L_0$. Electron spatial scales are distance between electrodes $2L_0$, sheath thickness L, electron free path λ, and distribution-tail energy relaxation length, $\lambda^* = \sqrt{\sigma/\sigma^*}\,\lambda$ (σ^* = inelastic cross section). Usually,

$$\omega_{0e} \gg \max\left(\sqrt{\nu\omega}, \omega\right). \qquad \omega \gg \nu^*. \qquad \nu \gg \nu^* \quad (1)$$

and the potential difference in the sheath U_0 considerably exceeds characteristic electron energies ε. From the condition $eU_0 \gg \varepsilon$, it follows that the moving boundary of the electron density profile is sharp compared with the sheath thickness L [1], [10]. If the first of the inequalities (1) holds, this moving boundary separates the quasi-neutral plasma with the low oscillatory field and the region of ion space charge with high field. So if $\omega_{0i} \ll \max\left(\omega, (\omega\nu_i)^{1/2}\right)$ [11], [12], where ν_i = ion collision frequency, the ion displacement during RF period is small, and for the calculation of the averaged field that determines the ion motion in the sheaths, it is convenient to introduce $z = \omega t(x)$—the equation of this moving boundary [1, eq. (18)]. From inequality $\omega \gg \nu^*$, the stationary of the EDF follows [13].

We restrict ourselves by the nonlocal case when the discharge dimension $2L_0$ is less than λ^* (the energy relaxation length for the bulk electrons λ_b considerably exceeds λ^* [14]). If λ_b is small compared with L_0, local approximation is valid when the EDF[1] can be factored to a form $n(x)f_v(v, \tilde{E}(x))$, and $f_v(v, \tilde{E}(x))$ is parametrically determined by the local value of oscillatory field $\tilde{E}(x)$. In the nonlocal case such an approach is erroneous, and if $L_0 \ll \lambda^*$, the EDF depends only on the combination $\varepsilon = mv^2/2 + e\phi(x)$. In the collision-

Manuscript received May 18, 1991; revised October 4, 1991.

The authors are with the Physics Technical Department, Leningrad State Technical University, St. Petersburg, Russia.

IEEE Log Number 9105985.

[1] By EDF we denote the particle density in the phase space that coincides with the probe current second derivative of the potential.

dominated case, $\lambda \ll (L, L_0)$, the standard two-term approximation for EDF is valid.

The EDF is determined by the energy gain from the electric field and energy loss in collisions. So even in the free-flight discharge where $\lambda \gg L_0$, the collision terms in the kinetic equation are important. If elastic collision frequency ν exceeds the inelastic one ν^* (1), the elastic collisions with small energy losses isotropize the EDF. Their direct influence on the energy balance is as a rule negligible for not too high pressures.

If $\omega \gg \Omega_b \gg \nu, L \ll \lambda$, the stochastic mechanism of electron heating by the sheath field is important. It has been proposed in [15] and explored by Goedde *et al.* [16] and Kushner [17]. We shall discuss this case in a forthcoming publication. Here, we consider the collisional nonlocal case $\lambda^* > L_0, L > \lambda$ when collisional heating dominates.

The nonuniformity of plasma is very important for the correct calculation of the EDF. In the quasi-neutral plasma, the ambipolar potential profile $\phi(x)$ always exists. That corresponds to the potential well for electrons. So the plasma electrons are trapped by this field and do not reach the peripheral region where the oscillatory field $\tilde{E}(x,t)$ and collisional heating are large. The nonlocal EDF in collisional and free-flight cases depends on the full energy $\varepsilon = mv^2/2 + e\phi(x)$ [14]. The steep decrease of the EDF tail produced by the inelastic collisions occurs at $\varepsilon > \varepsilon^*$ (ε^* = the first excitation potential). In the peripheral region, $\varepsilon = \varepsilon^*$ corresponds to kinetic energy values considerably less than ε^*. It means that the average excitation and ionization frequencies are significantly lower here than in the discharge center. As the time-averaged $\langle \tilde{E}^2(x) \rangle$ values (roughly proportional to $n_i^{-2}(x)$) are maximal in the peripheral region, the local approximation [1] gives the opposite dependence—the maximal excitation and ionization by the plasma electrons occur on the periphery. The nonlocal, collisional energy-diffusion coefficient is proportional to the space-time averaged $\langle \tilde{E}^2(x) \rangle$ and grows with ε. So in the collisional case the EDF slope steeply decreases with energy and the EDF is to be enriched by slow and fast electrons [18], [19]. The nonlocality condition $L \ll \lambda^*$ is equivalent to a limit of high thermal conductivity. So the widely used hydrodynamical description [20] also gives in this case an erroneous result of uniform mean electron energy and excitation (ionization) frequencies over the plasma cross section.

From exponential dependence of the ionization rate produced by plasma electrons I_1 on $\langle \tilde{E}^2(x) \rangle$, it follows that in the local α-regime, relatively small variations in plasma density lead to significant changes in the ionization rate $[I]$. Accordingly, the plasma density varies insignificantly and the main part of ion flux that reaches the electrode is generated in the sheath. On the contrary, in the nonlocal case the ion flux is generated in the central region; ionization in the plasma periphery and sheath (where $\tilde{E}$ is large) is negligible. So the ion density in the sheath falls steeply and the ion flux is almost constant here. Since the field at the electrode surface is determined by the current density j and is to be screened in the sheath by the ion space charge, the sheath thickness in the low-pressure discharge is considerably higher than in the high pressure one with the same current. The values of the dc potential difference in the sheaths are also higher in the nonlocal case.

Since the relaxation length of energetic γ-electrons far exceeds λ^* for plasma ones produced by the γ-electrons, ionization I_2 [1] in the nonlocal regime also occurs mainly in the plasma region. Its direct influence on the ion profile, opposite to the local case, is not very significant. The case with the contribution of I_2 dominating in the total ionization rate was discussed in [21]. Here, we neglect the ionization by γ-electrons, setting $\gamma = 0$.

In this paper a complete self-consistent equation for the above-described discharge is derived. It contains the electron kinetic equation, the equation for ion density, and the Poisson equation that in plasma takes the form of the quasi-neutrality equation $n_e = n_i$. In the ion space-charge region it can be also significantly simplified as $n_e = 0$ here, and the n_i profile is stationary.

In the second section the electron kinetic equation for the collisional nonlocal case with $\omega \gg \nu^*$ is investigated. The space-time-averaged kinetic equation obtained is sufficiently simple to be used in self-consistent calculations of RF discharges—it takes the form of the widely known one for the stationary and spatially homogeneous case; integrals of the unknown electric field profile appear in the coefficients of the averaged equation only. The third section deals with ion motion. Even in such simplified averaged form, the problem cannot be solved analytically and requires considerable numerical work. So here we present the problem formulation and results of qualitative investigation of the equation system. The fourth section is devoted to the comparison with the experiment. It is fulfilled in a comparatively crude approximation that can be treated as the first iteration of the self-consistent procedure. The detailed numerical modeling and its comparison with analytical approaches is in progress now and will be reported later.

II. Space-Time-Averaged Kinetic Equation for the EDF

It is widely known that the electric field in RF discharge is very inhomogeneous. It is small in the quasi-neutral plasma region, where $n_e \approx n_i$, that occupies the central part of the discharge, and it steeply rises in the ion space-charge part of the sheath region, with $n_e \approx 0$. The sharp transition region (its thickness is of the order of the Debye radius) [3], [10], [22] moves periodically between $x = \pm(L_0 - L) = \pm L_p$ and $x = \pm L_0$. We shall describe this boundary as a rigid moving wall $z(x)$ (Fig. 1). So in the point of the sheath $L_p < x < L_0$, electrons are present only in the plasma phase (between the times $t_1(x)$ and $t_2(x)$; Fig. 1(b)). In the plasma at $-L_p < x < L_p$, the time-averaged field is

$$\langle E(x) \rangle = \frac{\omega}{2\pi} \int_0^{2\pi/\omega} E(x,t)\, dt \tag{2a}$$

and the oscillatory part of the plasma field is

$$\tilde{E}(x,t) = E(x,t) - \langle E(x) \rangle. \tag{2a'}$$

In the sheath the averaged electric field in the plasma phase

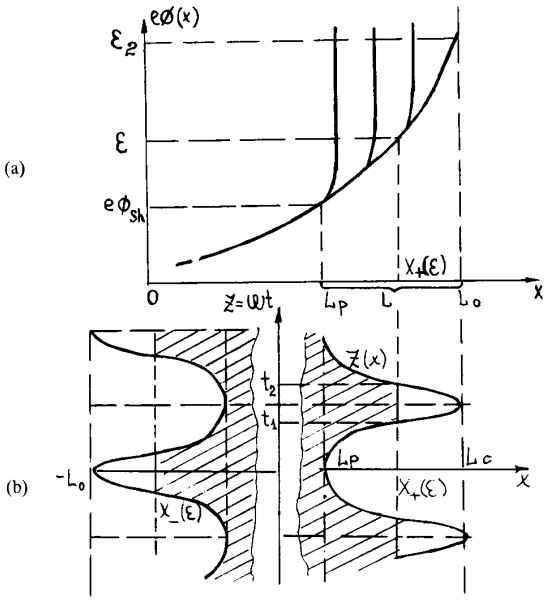

Fig. 1. (a) Schematic dependence of the averaged plasma electric potential (curve) and position of the plasma–space-charge boundary (vertical lines) at various times. (b) The plasma–space charge boundary motion in the sheath. Electrodes are at $|x| > L_0$.

that enters in the electron kinetic equation is [22]

$$\langle E(x)\rangle = \int_{t_1(x)}^{t_2(x)} E(x,t)\,dt/(t_2 - t_1). \tag{2b}$$

Introducing the potential energy $e\phi(x)$ that corresponds to the field ((2a) and (2b)), we can write the kinetic equation for the EDF $f(\vec{v},x,t)$ in the form:

$$\frac{\partial f}{\partial t} + v_x\frac{\partial f}{\partial x} - \left(\frac{e\tilde{E}}{m} + \frac{e\,d\phi}{m\,dx}\right)\frac{\partial f}{\partial v_x} = S(f) + S^*(f) \tag{3}$$

where x is the coordinate in the current direction, $\vec{v}$ is the electron velocity, $S(f)$, $S^*(f)$ are the elastic and inelastic collision integrals, and $\langle\tilde{E}\rangle = 0$.

If λ is small compared to the characteristic spatial scale, the two-term approximation is valid, $f(x,\vec{v},t) = F_0(\varepsilon,x,t) + F_1(\varepsilon,x,t)\cos(\vartheta)$, where ϑ is the angle between the electron velocity and x-axis between the directions of plasma inhomogeneity and RF current. The equation for $F_0(\varepsilon,x,t)$ in plane geometry is (J_x, J_ε = space and energy fluxes)

$$\nu\frac{\partial F_0}{\partial t} + \frac{\partial J_x}{\partial x} + \frac{\partial J_\varepsilon}{\partial \varepsilon} = \sum_k \nu\Big[-\nu_k^*(w)F_0(\varepsilon,x) + \frac{v_k}{v}\nu_k^*(w+\varepsilon_k)F_0(\varepsilon+\varepsilon_{k,x})\Big] \tag{4}$$

$$F_1 = -\frac{v\,\partial F_0}{(\nu+i\omega)\,\partial x} - \frac{e\tilde{E}v\,\partial F_0}{(\nu+i\omega)\,\partial\varepsilon} = \frac{3}{v^2}J_x; \qquad J_\varepsilon = e\tilde{E}J_x + \delta\nu\omega F_0 \tag{5}$$

where $\nu(w)$, $\nu_k^*(w)$ are the transport and excitation collision frequencies (dependent on the electron kinetic energy w), $\delta = 2m/M$, and ε_k is the excitation energy of level number k). If it is possible to neglect the energy losses in elastic collisions (second term in the expression for J_ε) and the last term in the right-hand side of (4) (it's determined by slow electrons that have lost energy ε_k in inelastic collisions and at not too high $\tilde{E}$ is significant only in the low-energy region), (4) has the form of a two-dimensional diffusion equation with coordinate-dependent diffusion coefficients and absorption coefficient $\sum\nu_k^* v = \nu^* v$.

Slow electrons with $\varepsilon < e\phi_{\rm sh}$ cannot reach the sheath boundary. So the boundaries $x_\pm(\varepsilon)$ that restrict their motion are time independent. Fast electrons ($\varepsilon > e\phi_{\rm sh}$) penetrate into the sheath during the plasma phase. The boundaries $x_\pm(\varepsilon)$ for the electrons are constructed from stationary and time-dependent parts (the available area for such electrons is dashed on Fig. 1(b)). The electrons' reflections from the moving part of these boundaries can lead to stochastic energy diffusion [15]–[17]. The boundary velocity $V \sim e\tilde{E}/m(\nu+i\omega)$ coincides with the electron drift velocity at the space-charge–plasma boundary. From $\nu \gg \nu^*$, it follows that chaotic velocity $v \gg V$ and the energy portion that transforms from directed into chaotic form in collisions with the boundary and with molecules are both of an order of $\Delta\tilde{\varepsilon}mvV$. As in the collisional regime where collisions of fast electrons with boundary are less frequent than with molecules, the energy diffusion coefficient $D_\varepsilon \sim \Delta\varepsilon^2\nu$ is determined by the latter process. Stochastic heating dominates in the opposite case—$D_\varepsilon \sim \Delta\varepsilon^2\Omega_b$. The $\tilde{E}$ values in the sheath exceed the plasma ones. So for the collisionless sheath, it is possible that fast electrons at the plasma periphery acquire directed energy mainly in collisions with the moving boundary, and transform it into the chaotic form in collisions with the neutrals [17]. If the nonlocality conditions $\lambda^* \gg L_0$ and $\omega \gg \nu^*$ are fulfilled, the energy relaxation is slow compared to spatial diffusion and $\tilde{E}(t)$ variation. So the isotropic part of EDF $F_0(\varepsilon,x,t)$ dependence is to be of the form:

$$F_0(\varepsilon,x,t) = f_0(\varepsilon) + f_0^{(1)}(\varepsilon,x,t) \tag{6}$$

where $f_0(\varepsilon)$ is the EDF $F_0(\varepsilon,x,t)$ space-time averaged over the dashed area on the Fig. 1. The small terms $f_0^{(1)} \ll f_0$ are determined by temporal and spatial inhomogeneity and are of an order of $(\nu^*/\omega)f_0$, $(L_0/\lambda^*)^2 f_0$ [13], [14]. Integrating the kinetic equation from $x_+(\varepsilon,t)$ to $x_-(\varepsilon,t)$ ($x_\pm(\varepsilon,t)$ are the equations of the left and right boundaries of the dashed region on Fig. 1—the coordinates of turning points for electrons with the total energy ε), we obtain:

$$\frac{\partial}{\partial t}\int_{x_-(\varepsilon,t)}^{x_+(\varepsilon,t)} vF_0\,dx + \Big[-vF_0\frac{\partial x}{\partial t} + J_x - J_\varepsilon\frac{\partial x}{\partial\varepsilon}\Big]_{x_-(\varepsilon,t)}^{x_+(\varepsilon,t)} + \frac{\partial}{\partial\varepsilon}\int_{x_-}^{x_+} J_\varepsilon(\varepsilon,x,t)\,dx = \int_{x_-}^{x_+} vS^*(F_0)\,dx. \tag{7}$$

Since energy relaxation at $\nu \gg \nu^*$ is slow, the directed electron velocity is small compared to the chaotic one ($F_0 \gg F_1$). So the position of real turning points differs insignificantly from $x_\pm(\varepsilon)$. For the stationary part of $x_\pm(\varepsilon, t)$ boundaries for fast electrons (and on the whole length of $x_\pm(\varepsilon)$ for slow ones), the first term in square brackets (7) vanishes and the last two terms, representing the particle source at $w = 0$, are equal to zero also. For the nonstationary parts of $x_\pm(\varepsilon, t)$, the sum of the first two terms in brackets in (7) equals zero—it is the flux at $x = x_\pm$ in the reference frame moving with the velocity $dx_\pm/dt$. As $dx_\pm/d\varepsilon = 0$ here, the expression in square brackets of (7) equals zero. So averaging (7) over time, we obtain a one-dimensional equation that formally coincides with the well-known local one:

$$\frac{d}{d\varepsilon}\overline{v\langle D_\varepsilon(\varepsilon)\rangle}\frac{df_0(\varepsilon)}{d\varepsilon} = \overline{\langle v\nu^*(\varepsilon)\rangle} f_0(\varepsilon) \tag{8}$$

where space-time averaging of the energy diffusion coefficient

$$D_\varepsilon(w, \varepsilon) = e^2 v^2 \nu \left\langle \tilde{E}^2(x)\right\rangle \Big/ \left[3\left(\omega^2 + \nu^2\right)\right] \tag{9}$$

and of excitation frequency $\nu^*(w)$ is to be performed according to

$$\overline{G(\varepsilon)} = \frac{1}{2L_0 T}\int_0^T \int_{x_-(\varepsilon)}^{x_+(\varepsilon,t)} G(\varepsilon - e\phi(x))\, dx\, dt\,. \tag{10}$$

For simplicity, the term with $\delta = 2m/M$ in (8) is neglected. So the EDF in this approach depends on the potential profile $\phi(x)$ only parametrically. The main distinctions between such nonlocal and traditional local approximations for the dc positive column were discussed in [14], [23], [24]. As in the dc case, the longitudinal electric field E_z does not depend on the coordinates, and the EDF in the local case can be factorized: $F_0 = n(r) f_0(v)$. So when the EDF is investigated by the standard probe method of measuring the second derivative $i'' = d^2 i/dU^2$ (i, U = the probe current and voltage), the functions $i''(U)$ in different points of discharge coincide if their arguments are shifted by the space potential in the probe position. In the nonlocal case, the unshifted functions $i''(U)$ coincide in different points of the tube cross section [24], [25]. The steep decrease of the EDF due to inelastic collisions begins at $\varepsilon = \varepsilon^*$ (excitation potential). In the peripheral points, this value corresponds to the kinetic energy w values that are considerably less than ε^* (Fig. 2). So in these points significant depletion of the EDF tail arises [25]. On the contrary, in the discharge center, tail depletion begins at $\varepsilon = w = \varepsilon^*$. But at a ε slightly exceeding ε^*, the discharge area where for the electron with a total energy ε value of $\nu^*(\varepsilon, x) \neq 0$ (dashed on the Fig. 2) is small compared to the entire available area (practically the entire discharge cross section). So the cross-section averaged value $\langle \overline{\nu\nu^*} \rangle$ is considerably less than in the local case—the EDF depletion "switches on" more softly. As near the excitation threshold $\nu^* \sim (w - \varepsilon^*)$ and the potential profile in the center is parabolic, the dependence

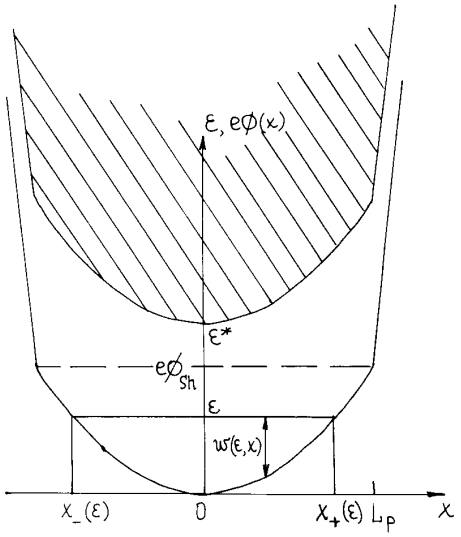

Fig. 2. Potential profile $\Phi(x)$ and electron energy plot for trapped electrons in discharge. Dashed area corresponds to the region in (ε, x) space, where inelastic collisions occur.

$\overline{\langle v\nu^*\rangle}(\varepsilon)$ in the vicinity of ε^* is $\sim(\varepsilon - \varepsilon^*)^2$ for cylindrical, and $\sim(\varepsilon - \varepsilon^*)^{3/2}$ for planar, geometry.

The second peculiarity of the nonlocal EDF in RF discharge arises from the averaging (10). As ion density $n(x)$ in the peripheral region is small, the RF field amplitude $\tilde{E}$ in the plasma phase which is roughly proportional to $n^{-1}(x)$ is large here. So for electrons with small energy ε which cannot reach this region, the averaged energy diffusion coefficient $\overline{\langle vD_\varepsilon\rangle}(\varepsilon)$ (9), (10) is small. On the contrary, high-energy electrons are penetrating into the high RF field region and their energy diffusion is large. Consequently, the EDF slope is large at low energies and diminishes with the energy growth. Such an EDF was observed in [18].

The complete equations system for electrons contains the kinetic equation (8), expressions for electron density

$$n_e(x) = \frac{4\pi}{m}\int_{e\varphi(x)}^{\infty} f_0(\varepsilon)\left[\frac{2}{m}(\varepsilon - e\phi(x))\right]^{1/2} d\varepsilon \tag{11}$$

and electron current density

$$j_e(x, t) = \frac{4\pi e^2 \tilde{E}(x, t)}{3m^2}\int_{e\varphi(x)}^{\infty} \frac{\varepsilon - e\phi(x)}{\nu + i\omega}\frac{df_0}{d\varepsilon}\, d\varepsilon = en_e V_e(x, t) = j_0 \sin\omega t. \tag{12}$$

The quasi-neutrality condition and the current conservation equation, together with (11) and (12), are connecting the dc and RF fields with the EDF.

In order to demonstrate the difference in spatial distribution of ionization produced by plasma electrons in the local and nonlocal cases, let us calculate the ionization frequency $\langle \nu_{\text{ion}}(x)\rangle$ averaged over time and EDF in different places of the plasma cross section. The excitation and

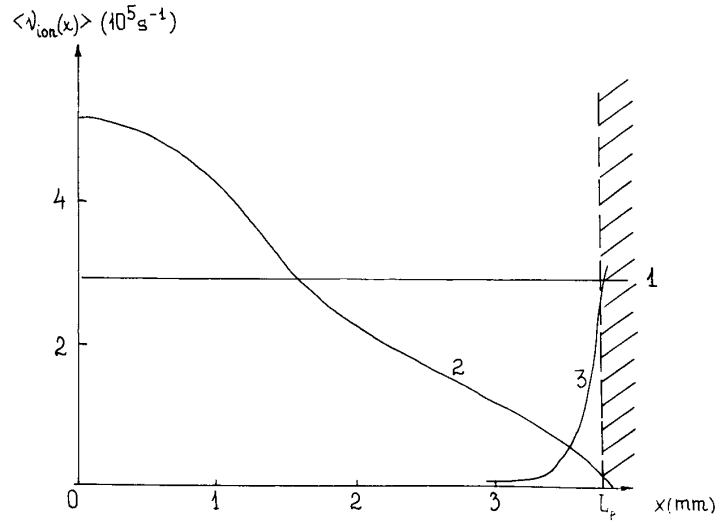

Fig. 3. Time-averaged ionization frequency in various points of model RF discharge in argon. (1) = Maxwell–Boltzmann; (2) = nonlocal approach, with $f_0(\varepsilon)$; and (3) = local approximation. The sheath is dashed.

ionization frequencies $v\nu^*$, $v\nu_{\rm ion}$ were laid proportional to $(w-\varepsilon^*)$, $(w-\varepsilon_i)$ with the coefficients that correspond to argon: $v\nu^* = g^*(w-\varepsilon^*)$; $v\nu_{\rm ion} = g_i(w-\varepsilon_i)$; $g^* = 2\cdot 10^{16}p(\mathrm{eV})^{-1}\,\mathrm{cm\,s^{-2}}$; $g = 4\cdot 10^{16}p(\mathrm{eV})^{-1}\,\mathrm{cm\,s^{-2}}$ (p = pressure (torr)). In the model case $\langle\overline{vD_\varepsilon}\rangle = \mathrm{const}(\varepsilon)$, the EDF at $\varepsilon < \varepsilon^*$ is

$$f_0 = A(\varepsilon_0 - \varepsilon) \tag{13}$$

where $\varepsilon_0 > \varepsilon^*$ is determined by the matching of (13) with the solution of (8) at $\varepsilon > \varepsilon^*$. The "absorbing wall" approximation $\nu^* \to \infty$ corresponds to $\varepsilon_0 \to \varepsilon^*$. At $\varepsilon > \varepsilon^*$, a steep decrease of the EDF occurs. The EDF part at $(\varepsilon - \varepsilon^*) < \varepsilon^*$ that corresponds to the majority of the inelastic collisions is of special interest. At such energies it is possible to use parabolic approximation of the dc potential profile $e\phi(x)$:

$$e\phi(x) = \varkappa\varepsilon^*(x/L_p)^2$$

where $L_p = (L_0 - L)$ = the plasma–sheath boundary position, $\varkappa \sim 1$. In the absorbing wall approximation, the EDF (13) corresponds to

$$T_e = \frac{2}{3}\int_0^{\varepsilon^*}\varepsilon^{3/2}(\varepsilon^*-\varepsilon)\,d\varepsilon \Big/ \int_0^{\varepsilon^*}(\varepsilon^*-\varepsilon)\sqrt{\varepsilon}\,d\varepsilon = \frac{2}{7}\varepsilon^*.$$

For crude estimate of the plasma density profile

$$n = n_0\cos(\pi x/2L_p)$$

and Boltzmann potential $\phi = (T_e/e)\ln(n/n_0)$, we have $\varkappa = \pi^2/28$.

According to (10), the inelastic collision-frequency averaging reduces to

$$\overline{\langle v\nu^*\rangle} = \frac{2}{3}g^*\frac{\varepsilon^*}{\sqrt{\varkappa}}(\varepsilon/\varepsilon^*-1)^q\frac{L_p}{L_0} \equiv \overline{\langle vD_\varepsilon\rangle}G(\varepsilon/\varepsilon^*-1)^q, \qquad q = 3/2. \tag{14}$$

At $\varepsilon^* \gg \varepsilon - \varepsilon^* > 0$, the EDF is

$$f_0 = (\varepsilon/\varepsilon^*-1)^{1/2}\mathrm{BK}_{1/(q+2)} \cdot \left[(\varepsilon/\varepsilon^*-1)^{(1+q/2)}\sqrt{G}/(1+q/2)\right] \tag{15}$$

where $\varepsilon_0 = \varepsilon^*(1+\beta/\varkappa)$,

$$\varkappa = \frac{\pi}{2\sin\frac{\pi}{2q}\Gamma\left(\frac{q+3}{q+2}\right)}\left(\frac{\varepsilon^{*q+2}G}{(q+1)^2}\right)^{1+q/2}$$

$$\beta = \frac{\pi}{2\sin\frac{\pi}{2q}\Gamma\left(\frac{q+1}{q+2}\right)}\left(\frac{(q+1)^2}{\varepsilon^{*q+2}G}\right)^{1+q/2}, \qquad B = A\varepsilon_0/\varkappa.$$

The local case corresponds to $q = 1$. The time-averaged over the EDF (15) direct-ionization frequency $\langle\nu_{\rm ion}(x)\rangle$ is presented in Fig. 3. We took $vD_\varepsilon = 2\cdot 10^{14}\langle\tilde{E}^2(x)\rangle/p$, that corresponds to argon at $\omega \ll \nu$. The model discharge was characterized by $2L_0 = 1.6$ cm, $j_0 = 8.2\ \mathrm{mA/cm^2}$, $p = 0.1$ torr, and $\omega = 13.56$ MHz. Self-consistent values of $U = 715$ V, $n_0 = 2\cdot 10^{10}\ \mathrm{cm^{-3}}$, and $L = 0.42$ cm were found using the calculated $\langle\nu_{\rm ion}(x)\rangle$ profile according to Sections III and IV.

The ion density profile in the discharge gap and the $\tilde{E}(x)$ dependence in the quasi-neutral region were calculated using the Maxwell–Boltzmann EDF according to [12], [26]. The electron temperature was determined by the energy balance and was found to be 2.5 eV. With this $\tilde{E}(x)$ profile, local and nonlocal EDF were calculated; the dependence $\langle\tilde{E}^2(\overline{x})\rangle$ on ε in the nonlocal case was neglected and the value corresponding to $\varepsilon = \varepsilon^*$ was taken. Surprising is the close coincidence of Maxwell–Boltzmann and nonlocal kinetic results. The nonlocality of the EDF criterion is equivalent to the limit of high thermal conductivity. So this coincidence is of the same origin as that one noted in [20] and [27] of hydrodynamic and kinetic results. The local approximation leads to $\langle\nu_{\rm ion}\rangle$ values in the discharge orders of magnitude lower than kinetic ones.

Self-consistent numerical simulation of the simplified model for such a nonlocal discharge was performed in [8]. The main differences with Fig. 3 are that $n(x)$, $\langle\nu_{\rm ion}(x)\rangle$ profiles in [8] were almost flat in the plasma region, and the EDF was enriched by slow electrons. The main reason of these discrepancies to our opinion is the approximation of constant $\langle\nu D_\varepsilon\rangle$ used in our calculation (see below). The transition from the local to nonlocal regime with pressure decrease was also observed in [8]. It was accompanied by the shift of the plasma source from the sheath-adjacent region to the plasma center; the central plasma density for a given current value was almost pressure independent. Accordingly, the ion flux from plasma decreases in the nonlocal case, and the sheath thickness considerably increases.

III. Ion Motion

The ion motion in the collision-dominated regime at $\omega \gg \omega_{0i}^2/\nu_i$ was analyzed in [12]. In plasma it is determined by the system:

$$\frac{d}{dx}nU = \langle\nu_{\rm ion}\rangle n: \quad n(x) = \frac{4\pi\sqrt{2}}{m^{3/2}}\int\limits_{e\phi(x)}^{\infty} f_0(\varepsilon)\sqrt{\varepsilon - e\phi(x)}\,d\varepsilon$$

$$MU^2 = \frac{2ed\phi}{\pi\,dx}\lambda_i. \tag{16}$$

Since ionization in the plasma–sheath boundary vicinity is negligible, the ion flux from plasma $\Gamma = nU|_{x=L_p}$ can be found with a zero-boundary condition for plasma density $n(x = L_p) = 0$.

The system (16) can be easily solved for three limiting cases:

a) The Maxwell–Boltzmann EDF for all electrons:

$$\phi = -\frac{T_e}{e}\ln(n/n_0); \qquad \langle\nu_{\rm ion}\rangle = {\rm const}(x)$$

$$2\pi x\Big/\left(3\sqrt{3L_p}\right) = \frac{1}{3}\left\{\frac{1}{2}\ln\frac{\left(1+\tilde{U}\right)^2}{\tilde{U}^2-\tilde{U}+1} + \sqrt{3}\,{\rm arct}\,g\frac{2\tilde{U}-1}{\sqrt{3}}\right\} + \frac{\pi}{6\sqrt{3}} \equiv x/x^*$$

$$n = n_0\left(1+\tilde{U}^3\right)^{-1/3}$$

$$\tilde{U} = U\left(\frac{3\sqrt{3}(ML_p)}{4\lambda_i T_e}\right)^{1/2} \equiv U/U^* \tag{17}$$

where U^* = the characteristic ion velocity in plasma. From (17) the ion flux at the plasma–sheath boundary is determined by

$$\Gamma = n_0 U^*. \tag{18}$$

b) $\langle\nu_{\rm ion}\rangle n = {\rm const}$. This case corresponds to a situation when the majority of electrons are slow [9]. Now the $\phi(x)$ profile in plasma is determined by their small energy, and influence of this field on the fast electrons that are responsible for ionization rate is negligible. So the ionization $\langle\nu_{\rm ion}\rangle n$ in this case is x-independent. We suppose for simplicity that slow electrons have the Maxwell–Boltzmann EDF:

$$n(x) = n_0\left(1-(x/L_p)^3\right)^{1/2}$$

$$\langle\nu_{\rm ion}\rangle n = \left(\frac{T_e}{ML_p}\frac{\lambda_i}{\pi}\right)^{1/2} n_0$$

$$\Gamma = nU|_{x=L_p} = \left(\frac{3}{\pi}\frac{T_e\lambda_i}{ML_p}\right)^{1/2} n_0. \tag{19}$$

As nonlocality leads to a peaked profile of $\langle\nu_{\rm ion}(x)\rangle$, it's useful to consider the limiting case of c).

c) $n\langle\nu_{\rm ion}(x)\rangle = \Gamma\delta(x)$. The ion flux in plasma $nU = \Gamma$ is constant. If the bulk electrons have the Maxwell–Boltzmann EDF, the plasma profile is $n \sim \exp(-e\phi/T_e)$. From (16) we have

$$2T_e\lambda_i/M\frac{d\ln n}{dx} = \pi\Gamma^2.$$

So

$$n_0^2 - n^2 = \frac{\pi M}{T_e\lambda_i}\Gamma^2 x \tag{20}$$

and

$$\Gamma = n_0\sqrt{\frac{T_e\lambda_i}{\pi ML_p}} \tag{21}$$

differ from (19) only by the factor $3^{-1/2}$. Since b) and c) represent the limiting cases of ionization spatial inhomogeneity, the real dependence between n_0 and Γ is between (18) and (20). For the ion profile in the sheath we have [1], [10], [12]

$$\frac{dz}{dx}\sin z = \frac{e\omega\Gamma}{Uj_0}$$

$$U(x) = \left(\frac{8\lambda_i j_0}{\omega M}\right)^{1/2}\int\limits_0^{z(x)}(\cos z' - \cos z)^{1/2}\,dz'/\pi. \tag{22}$$

From (22) we have for the sheath thickness

$$L = \frac{0.9j_0}{e\omega n_{\rm sh}}$$

where the ion density at the electrode surface is

$$n_{\rm sh} = 1.1\Gamma\left(\frac{\omega M}{8e\lambda_i j_0}\right)^{1/2}. \tag{23}$$

The density in the sheath is of the order of $n_{\rm sh}$:

$$\int\limits_{L_p}^{L_0} n\,dx = 2.2n_{\rm sh}L.$$

The density profile in plasma (20) and the sheath (22) together with (11) and (12) determine the oscillatory field profile $\tilde{E}(x,t)$. Calculating the source term $\langle\nu_{\rm ion}\rangle n$ with the EDF (8) completes the self-consistent problem formulation. So

contrary to the local case [1], the main discharge characteristics are nonsensitive to the value of n_b—the ion density at the plasma–sheath boundary $x = L_p$. The ionization rate and ion flux Γ can be found from the diffusion equations (16), (19)–(21), with a zero boundary condition, and the ion profile in the main part of the sheath is determined by (22), where the diffusion is neglected. Nevertheless, since some discussion took place and discrepancies exist between the n_b values given by [1], [10], [12] and since the system (22) leads to discontinuity of the density profile at $z = 0$, we will treat this problem in some detail.

In [1], [22], it was demonstrated that in the vicinity of the plasma–sheath boundary the transition region exists where the averaged fields of thermal (diffusion) and nonthermal origin are comparable. The width of this region is

$$\delta \sim \left(\frac{ej_0 r_D}{\omega T_e}\right)^{1/5} r_D \gg r_D, \qquad \delta \ll L_p$$

where $r_D(n_b)$ = the Debye radius in the transition region. So the junction of the diffusion-dominated plasma profile and (22) can be performed precisely in the standard boundary layer scheme. If we want, as it is usually done, to match the plasma profile and (22) in some point $x = L_p$, $n = n_b$, an error of order of unity arises in the transition region. In our opinion, the simplest way to do so is to define the boundary position in the point where U values obtained from the plasma equations and from (22) coincide. It corresponds to the choice of the boundary position in the point that is situated at a distance δ (extrapolated length) from the point where the diffusion profile $n(x) = 0$. The sheath profile (22) begins from the corresponding values z_b, U_b. In these terms the procedures proposed in [10] (where the extrapolated length instead of δ was chosen as $r_D(n_b)$) and [12] (where the Bohm criterion for the collisional case was postulated) can lead to a more significant error in the transition region compared to the proposed scheme. If the value of δ (21) is small compared to λ_i, the Bohm criterion for n_b is valid.

IV. The Comparison with Experiment

A detailed investigation of the EDF in Ar and He was performed in [9], [28] at the pressure range of $0.1 \div 3$ torr at a frequency of 13.56 MHz and discharge gap $2L_0 = 6.7$ and 2 cm. The characteristic sheath thickness was of an order of 1 cm. It corresponds to the collisional local and nonlocal cases. So stochastic heating doesn't in our opinion play a significant role in most of the experiments [9], [28]. Let us compare the derived formulae with the experiment. In the high-pressure case a local EDF is formed. For example, at $p = 3$ torr, $2L_0 = 2$ cm, and $j_0 = 2.8\ \mathrm{mA/cm^2}$, the electron density in the plasma center was $0.6 \cdot 10^{10}\ \mathrm{cm^{-3}}$ and the plasma oscillatory electric field amplitude according to (12) is $\tilde{E}_0 = 24$ V/cm. For energy gain from zero to $\varepsilon^* = 11.5$ eV, the time $\tau = (2\varepsilon^*/\pi)^2/D_\varepsilon \sim 0.4\ \mu$s is required, where D_ε is given by (9). The spatial displacement during τ is $(4D\tau)^{1/2} \sim 2.4 \cdot 10^{-1}$ cm—small compared to the characteristic space scale $(2L_0/\pi)$. The displacement of energetic electrons with $w \cong 13$ eV during the inelastic collision time—ν^{*-1} equals

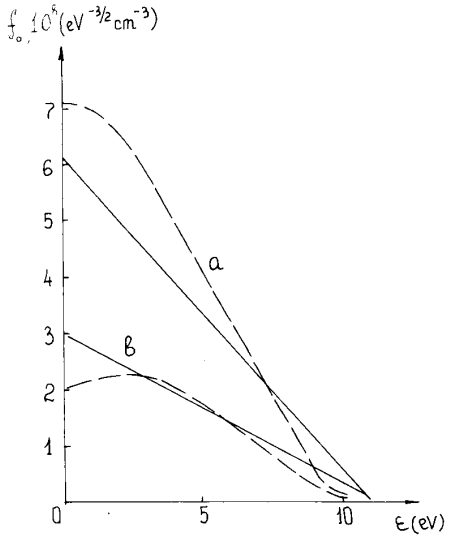

Fig. 4. The local EDF for argon: (a) $f = 13.6$ MHz, $j_0 = 2.8\ \mathrm{mA/cm^2}$, $p = 3$ torr, $2L_0 = 2$ cm; (b) $f = 13.6$ MHz, $j_0 = 1.0\ \mathrm{mA/cm^2}$, $p = 1$ torr, $2L_0 = 6.7$ cm. Dashed lines = experiment [9] and solid lines = calculation.

to $(4D/\nu^*)^{1/2} \sim 1.7 \cdot 10^{-2}$ cm—also is small compared to $2L_0/\pi$. As energy losses in elastic collisions are negligible, the isotropic EDF is determined by the local equation:

$$\frac{\partial}{\partial w} v D_\varepsilon(w, x) \frac{\partial f_0}{\partial w} + v\nu^*(w) f_0 = 0$$

that formally coincides with (8). The only distinction from the solution (13), (15) consists in replacing ε with w and $q = 3/2$ with unity.

The approximation $(v^3/\nu) = \text{const}$ was used for argon. Figs. 4 and 5 present the local EDF in the discharge center for the absorbing wall approximation $\nu^* \to \infty$ with $\omega = 2\pi \cdot 13.56\ \mathrm{s^{-1}} \ll \nu$, $j_0 = 2.8\ \mathrm{mA/cm^2}$, $\rho = 3$ torr, $2L_0 = 2$ cm (a), and $j_0 = 1\ \mathrm{mA/cm^2}$, $\rho = 1$ torr, $2L_0 = 6.7$ cm (b). The values of $\tilde{E}$ profile were determined according to (12) using experimental n_0 values. The discrepancy at higher pressure (a) is mainly due to energy losses in elastic collisions.

In these calculations we ignored the nonzero energy values after inelastic collisions (second term in the right-hand side of (5)).

Calculation of the nonlocal EDF is a far more difficult problem than the local one, because the EDF now depends on the entire density and potential profile. We restrict ourselves here by the purely collisional case L_p, $L \gg \lambda$. The cases L, $L_p \ll \lambda$, when the stochastic heating dominates, and $L < \lambda < L_p$, when fast electrons gain energy from oscillating sheathes and dissipate it collisionally, will be discussed elsewhere.

We consider the case $e\varphi_{\mathrm{sh}} < \varepsilon^*$; this inequality holds as in reported in [9], [28] experiments. For qualitative description we assume the following model for the spatially averaged energy diffusion coefficient (9):

$$D(\varepsilon) = \langle \overline{vD_\varepsilon} \rangle = \frac{e^2 \nu(\varepsilon) \varepsilon^{3/2}}{6(\omega^2 + \nu^2(\varepsilon))} \left(\frac{2}{m}\right)^{3/2}$$

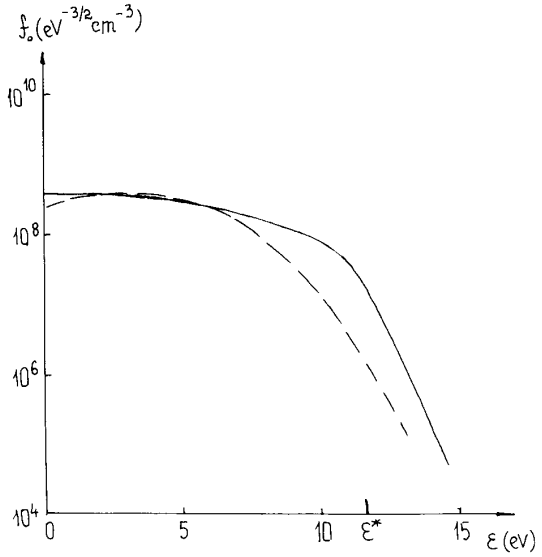

Fig. 5. The local EDF for argon for the same conditions as in Fig. 4(b).

$$* \begin{cases} \overline{\tilde{E}_s^2} \\ \tilde{E}_f^2 \end{cases} \equiv \begin{cases} D_s \text{ at } \varepsilon < \varepsilon_b \\ D_f \text{ at } \varepsilon > \varepsilon_b \end{cases} \tag{24}$$

where the boundary energy between slow and fast parts of EDF $\varepsilon_b > e\varphi_{\rm sh}$ is defined by

$$n(\varepsilon_b) = 4\pi\sqrt{2}/m^{3/2} \int_{\varepsilon_b}^{\infty} f_0(\varepsilon)\sqrt{\varepsilon - \varepsilon_b}\, d\varepsilon$$

$$= n_{\rm sh} = 1.1 n_0 \left(\sqrt{\frac{\omega T_e}{4\pi e L_p j_0}} \right)^{1/2} \tag{25}$$

where $n_{\rm sh}$ is defined by (23), and expression (20) is used. The square of averaged-oscillatory electric field slow and fast electrons is determined by the simplified current conservation equation $\tilde{E}(x,t) = \tilde{E}_0 n_0 \cos(\omega t)/n(x)$ instead of (12), and by the real density profile (19) in the plasma and uniform density (23) in the sheath. Such an approximation is based on the fact that in the investigated cases, the ratio n_0/n_b was of an order of 10, while the ratio $n_b/n_{\rm sh}$ didn't exceed 3.

So we have

$$\left\langle \overline{\tilde{E}_s^2} \right\rangle = 0.4\tilde{E}_0^2 [1 + \ln(n_0/n_b)]^{L_p}/L_0$$

$$\left\langle \overline{\tilde{E}_f^2} \right\rangle = 0.082 \left(\frac{\tilde{E}_0 n_0}{n_{\rm sh}} \right)^2 L/L_0. \tag{26}$$

Since the slow electrons' energy diffusion coefficient is small $(D_s/D_f \sim (n_{\rm sh}/n_0)^2 L_0/L \sim j_0^{-3/2} \ll 1)$, they are retarded at low ε, where values of D_ε are small [29]. The electron energy flux

$$\Gamma_\varepsilon = D \frac{\partial f_0}{\partial \varepsilon}$$

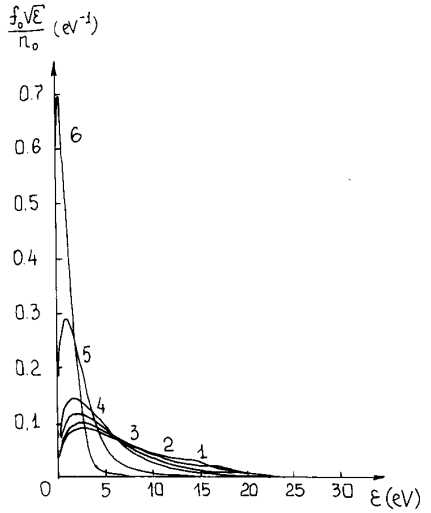

Fig. 6. The experimental normalized values $(f_0\sqrt{\varepsilon}/n_0)$ [28] are plotted for He at $f = 13.6$ MHz, $p = 0.1$ torr, and $2L_0 = 6.7$ cm. The current density values (mA/cm^2) are: (1) $= j_0 = 0.085$; (2) $= 0.22$; (3) $= 0.58$; (4) $= 1.3$; (5) $= 3.0$; and (6) $= 8.8$.

at $\varepsilon < e\varphi_{\rm sh}$ is conserved. So the ratio of the EDF slope at $\varepsilon > e\phi_{\rm sh}$ to the one at $\varepsilon > e\phi_{\rm sh}$ increases with current as $\sim j_0^{3/2}$. In Fig. 6 experimental values of $f_0\sqrt{\varepsilon}$ in He for different currents are shown. The EDF slope at low energies steeply increases with j_0.

Such an approach overestimates the energy diffusion of slow electrons (as the average field square is replaced by its maximal value (26)). But at low energies in the experimentally investigated situations, the electron–electron collisions dominate, forming the Maxwellian EDF here.

For an approximate account of the electron–electron collisions, we use the collision integral for fast electrons with Maxwellian ones [30]. In two-term approximation, it reduces to

$$S_0^{(ee)} = -\frac{m}{v}\frac{\partial}{\partial \omega}\left\{ v^3 \left[\nu_{ee}\left(f_0 + T_e \frac{\partial f_0}{\partial \omega} \right) \right] \right. \tag{27}$$

where

$$\nu_{ee} = \frac{4\pi n_e e^4 \ln \Lambda}{m^2 v^3}$$

is the Coulomb collision frequency. The error of (27) is maximal when the distribution of slow electrons is non-Maxwellian, but in such a case this term in the kinetic equation (8) is small.

For experimental conditions $p = 0.1$ torr Ar, $j_0 = 2.65$ mA/cm^2, $2L_0 = 2$ cm using the experimental value $n_0 = 1.3 * 10^{18}$ cm^{-3}, we have from (22), (23) $n_{\rm sh} = 0.66 \cdot 10^9$ cm^{-3} and $L = 0.26$ cm, which is close to the experimental values.

The characteristic fast-electron energy relaxation time $\tau_{\varepsilon f} = \varepsilon^{*2}/D_f \sim 2.5 \cdot 10^{-6}$ s is small compared to $\nu_{ee}^{-1} = 2 \cdot 10^{-5}$ s. On the contrary, $\tau_{es} \sim 2.5 \cdot 10^{-4}$ s for slow electrons near the Ramsauer minimum considerably exceeds ν_{ee}^{-1}. So the

approximate averaged kinetic equation instead of (8) is $\left(D_e = mT_e\overline{v^3\nu_{ee}}\right) = \text{const}(\varepsilon)$.

$$-(D_s + D_e)\frac{\partial f_0}{\partial \varepsilon} - D_e f_0/T_e = \Gamma_\varepsilon, \qquad \text{at } \varepsilon < \varepsilon_b$$

$$-D_f\frac{\partial f_0}{\partial \varepsilon} = \Gamma_\varepsilon, \qquad \text{at } \varepsilon_b < \varepsilon < \varepsilon^*.$$

The EDF in the absorbing wall approximation $f_0(\varepsilon^*) = 0$ for energy-independent D_e, D_s is as indicated in (28), below.

As in the electron–electron collisions energy is conserved, T_e is determined by

$$\int_0^{\varepsilon_b} D_s\frac{\partial f_0}{\partial \varepsilon}\,d\varepsilon = \Gamma_\varepsilon\varepsilon_b. \tag{29}$$

We assume the approximation

$$\nu(\varepsilon) = \begin{cases} 4.8\cdot 10^8 p\varepsilon^{3/2}, & \text{at } \varepsilon_b < \varepsilon \\ 3.8\cdot 10^7 p\varepsilon^{1/2}, & \text{at } \varepsilon_b > \varepsilon \end{cases} \tag{30}$$

where ε is in electronvolts, and p is in torr. From $v_{ee}\tau_{es} \gg 1$, it follows that $D_e \gg D_s$. So from (28) and (29) we have for T_e, ε_b:

$$\left(\frac{T_e}{\varepsilon^*}\right)^{5/2} = \frac{n_0}{n_{sh}}\frac{16}{15}\frac{T_e}{\sqrt{\pi}\varepsilon_b}\frac{D_s}{D_f}\frac{(T_e)}{(\varepsilon^*)}$$

$$e^{-\varepsilon_b/T_e} = \frac{2T_e D_s(T_e)}{\varepsilon_b D_e(T_e)}. \tag{31}$$

From (31) it follows that $T_e = 0.037\varepsilon^* = 0.42$ eV; and $\varepsilon_b = 3.44T_e = 1.40$ eV. In Fig. 7, calculated electron–electron collisions and the experimental EDF are plotted. The qualitative agreement is clearly seen. The coincidence of the EDF tail at $\varepsilon \gtrsim \varepsilon^*$ demonstrates that the numerical value of the energy diffusion coefficient (24) is close to the real one. The sharp knee between slow and fast parts of the calculated EDF is mainly due to the step-wise approximation (24). The role of the electron–electron collisions is demonstrated in Fig. 8, where the calculated EDF for the same conditions with and without electron–electron collisions is presented. The EDF for fast electrons (28) for argon is close to (13), and the maximum on the calculated $f_0\sqrt{\varepsilon}$ arises at $\varepsilon = \varepsilon^*/3$.

As in He, the Ramsauer effect is absent, and the EDF slope ratio at low and high energies for equal currents is less than in the case of Ar. The effect of growth of the relative number of slow electrons with current is less pronounced here. Fig. 6 demonstrates that the enrichment of the low energy part of the EDF in He also grows with current. The enrichment of the slow part of the EDF in the absence of the Ramsauer effect is also demonstrated by the calculations [8].

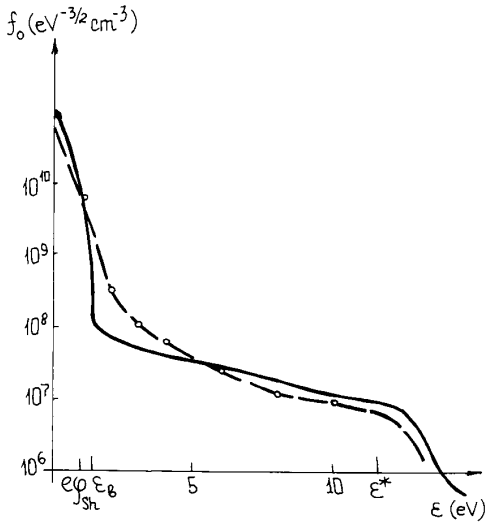

Fig. 7. The experimental [9] (dashed) and calculated (solid) EDF for argon: $f = 13.6$ MHz; $2L_0 = 2$ cm, $j_0 = 2.7$ mA/cm^2, and $p = 0.1$ torr.

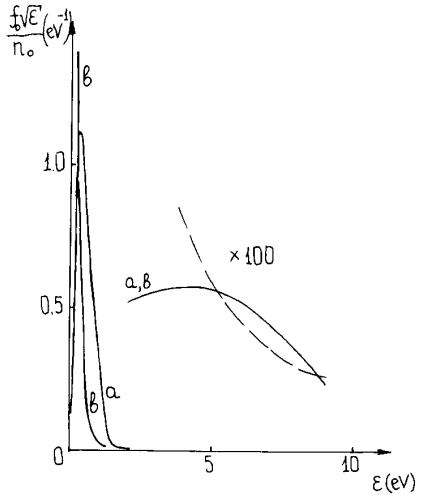

Fig. 8. The experimental [9] (dashed) and calculated (solid) normalized EDF for the same conditions as in Fig. 7: (a) with e–e collisions; and (b) without e–e collisions.

ACKNOWLEDGMENT

The authors are grateful to Dr. V. A. Godyak for encouraging this work and for his continuing advice. They are also grateful to the referees for their helpful criticism.

$$f_0 = \begin{cases} T_e\Gamma_\varepsilon/D_e\left[-1 + \exp\left[\frac{(\varepsilon_b-\varepsilon)/D_e}{T_e(D_e+D_s)}\right]\left(1 + D_e/T_e\int_{\varepsilon_b}^{\varepsilon^*}\frac{d\varepsilon'}{D_f(\varepsilon')}\right)\right], & \text{at } \varepsilon < \varepsilon_b \\ \Gamma_\varepsilon\int_{\varepsilon}^{\varepsilon^*}\frac{d\varepsilon'}{D_f(\varepsilon')}, & \text{at } \varepsilon > \varepsilon_b. \end{cases} \tag{28}$$

REFERENCES

[1] A. S. Smirnov and L. D. Tsendin, in *IEEE Trans. Plasma Sci.*, vol. 19, pp. 130–140, Apr. 1991.
[2] E. A. Volkova *et al.*, in *Sov. J. Plasma Phys.*, vol. 16, no. 6, pp. 738–745, 1990.
[3] V. A. Godyak, *Soviet Radio Frequency Discharge Research.* Falls Church, VA: Delphic Assoc., 1986.
[4] R. W. Boswell and I. J. Morey, in *Appl. Phys. Lett.*, vol. 52, pp. 21–23, 1988.
[5] M. Surendra, D. B. Graves, and I. J. Morey, in *Appl. Phys. Lett.*, vol. 56, no. 11, pp. 1022–1024, 1990.
[6] D. Vender and R. W. Boswell, in *IEEE Trans. Plasma Sci.*, vol. 18, pp. 725–733, Aug. 1990.
[7] T. J. Sommerer, W. N. G. Hitchon, and J. E. Lawler, in *Phys. Rev. Lett.*, vol. 63, pp. 2361–2364, 1989.
[8] D. B. Graves and M. Surendra, in *Proc. SPIG* (Dubrovnik, Yugoslavia), 1990.
[9] V. A. Godyak and R. B. Piejak, in *Phys. Rev. Lett.*, vol. 65, pp. 996–999, 1990.
[10] V. A. Godyak and N. Sternberg, in *Phys. Rev.*, vol. A42, pp. 2299–2312, 1990.
[11] V. A. Godyak and A. S. Khanneh, in *Sov. J. Plasma Phys.*, vol. 5, pp. 376–380, 1979.
[12] M. A. Lieberman, in *IEEE Trans. Plasma Sci.*, vol. 17, pp. 338–341, 1989.
[13] L. D. Tsendin, in *Sov. Phys.*, vol. 47, no. 8, pp. 925–928, 1977.
[14] L. D. Tsendin, in *Sov. Phys. JETP*, vol. 39, no. 4, pp. 805–810, 1974.
[15] V. A. Godyak, in *Sov. J. Plasma Phys.*, vol. 2, pp. 141–151, 1976.
[16] C. G. Goedde, A. J. Lichtenberg, and M. A. Lieberman, in *J. Appl. Phys.*, vol. 64, no. 9, pp. 4375–4382, 1990.
[17] M. Kushner, in *J. Appl. Phys.*, vol. 54, pp. 4958–4965, 1983; see also, *IEEE Trans. Plasma Sci.*, vol. PS-14, pp. 188–194, 1986.
[18] V. A. Godyak and S. N. Oks, in *Sov. Phys.–Tech. Phys.*, vol. 24, no. 10, pp. 1255–1256, 1979.
[19] I. D. Kaganovich and L. D. Tsendin, in *Proc. VIII ESCAMPIG* (Orleans, France), 1990, pp. 161–162.
[20] G. Roumeliotis and L. E. Cram, in *J. Phys. D.*, vol. 22, pp. 113–119, 1989.
[21] V. A. Godyak and A. S. Khanneh, in *IEEE Trans. Plasma Sci.*, vol. PS-14, pp. 112–123, 1986.
[22] L. D. Tsendin, in *Sov. Phys.–Tech. Phys.*, vol. 35, no. 8, pp. 904–907, 1990.
[23] I. B. Bernstein and T. Holstein, in *Phys. Rev.*, vol. 94, pp. 1475–1482, 1954.
[24] L. D. Tsendin and Yu. B. Golubovsky, in *Sov. Phys.–Tech. Phys.*, vol. 22, pp. 1066–1073, 1977.
[25] D. Herrman, A. Rutcher, and S. Pfau, in *Beit. Plasma Phys.*, Bd. 11, pp. 75–87, 1971.
[26] I. D. Kaganovich and L. D. Tsendin, in *Sov. Phys. Tech. Phys. Lett.*, vol. 16, no. 2, pp. 46–48, 1990.
[27] L. E. Kline and M. J. Kushner, *Solid-State Mater. Sci.*, vol. 16, pp. 1–35, 1989.
[28] V. A. Godyak, presented at ICPIG, Pisa, Italy, 1991 (invited lecture); see also, V. A. Godyak, private communication.
[29] L. D. Tsendin, *Sov. Phys.–Tech. Phys.*, vol. 41, no. 11, p. 2271, 1971.
[30] A. V. Gurevich and A. B. Shwarzburg, *Non-Linear Theory of Radiowaves Propagation in the Ionosphere* (in Russian). Moscow: Nauka, 1973.

Igor D. Kaganovich was born in Leningrad, USSR, in 1966. He received the engineer-physicist diploma (equivalent of the M.S. degree) in hydrodynamics from the Leningrad Polytechnic Institute in 1989.

He is currently working on the physical problems of RF plasma discharges at the Physics and Technology Faculty of the Leningrad State Technical University.

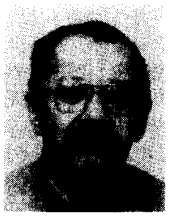

Lev D. Tsendin was born in Leningrad, USSR, in 1937. He graduated from the Leningrad State University in 1959 in theoretical physics. He was a candidate in physical-mathematical sciences (theoretical physics) in 1969, and received the doctor of physical-mathematical sciences (physics and chemistry of plasma) degree in 1982.

Since 1964 he has been at the Leningrad Polytechnic Institute (now the Leningrad Technical University), where he is a Principal Scientist and full Professor in the Physical Technical Department (plasma physics). His principal professional interests include plasma theory, transport phenomena in plasma, plasma kinetics, and RF and dc gas discharges.